Office of Naval Research Grant N00014-98-I-0115
"Analysis of Acoustic Propagation, Bubble Field and Environmental Data from the Scripps Inshore Bubble Field Experiment"
1 November 1997 to 31October 1998

Final Technical Report
1 June 1999

Principal Investigator: David Farmer
Institute of Ocean Sciences
P.O. Box 6000
Sidney B.C. V8L 4B2 CANADA

Introduction:

This project represents a first step towards understanding the role of bubbles in modifying acoustic propagation in the surf zone. Our component of the project involved carrying out detailed bubble measurements, along with other oceanographic observations. The bubble field is explained in terms of oceanographic processes. Providing a basis for future modeling of high frequency acoustic propagation. Moreover, preliminary propagation measurements were acquired at the same time (see attached report on the experiment). Subsequent analysis of the propagation measurements will use results of the present study in a combined bubble-advection/diffusion and propagation analysis.

Acoustical telemetry between divers or unmanned vehicles and mother ships further offshore requires understanding of the processes affecting sound propagation in the area of interest. Interactions with the sea bed and the sea surface play major roles in surf zone sound propagation but also bubbles generated by breaking surf and carried seaward by turbulent flows and rip currents will influence the sound field significantly. Because of the high Q of bubbles the frequency dependent attenuation and scattering of sound by bubbles are strongly dependent on the size distribution of the bubbles as well as the spatial distribution.

The mean offshore flow, or rip current, is a relatively strong current which compensates for the shoreward mass transport in the breaking wave crests. Dyhr-Nielsen and Soerensen (1970) were the first to describe the phenomenon theoretically. They argued that the rip current is caused by the local imbalance between the depth varying momentum flux and the depth uniform set-up force. These rip currents represent the dominant mechanism for moving bubbles and sediments away from the actively breaking zone and offshore. Bubbles moved by these rip currents will rise through the water column because of their buoyancy and they will shrink or increase in size due to differences in partial pressures inside and outside the bubbles. These effects will significantly alter the bubble size distribution with time and reduce the overall air-fraction. However, measurements of bubble concentrations between 55m and 220m offshore from the active breaking zone and at depths of up to 4m below the surface show

REPORT DOCUMENTATION PAGE

Form Approved
OMB No. 0704-0188

1. REPORT DATE *(DD-MM-YYYY)*	2. REPORT ~~DATE~~ TYPE	3. DATES COVERED *(From - To)*
22-07-1999	FINAL TECHNICAL	NOV 1997 – OCT 98

4. TITLE AND SUBTITLE
Analysis of Acoustic Propagation, Bubble Field and Environmental Data from the Scripps Inshore Bubble Field Experiment.

5a. CONTRACT NUMBER

5b. GRANT NUMBER
N00014-98-1-0115

5c. PROGRAM ELEMENT NUMBER

6. AUTHOR(S)
Farmer, David, M

5d. PROJECT NUMBER

5e. TASK NUMBER

5f. WORK UNIT NUMBER

7. PERFORMING ORGANIZATION NAME(S) AND ADDRESS(ES)
INSTITUTE OF OCEAN SCIENCES
9860 WEST SAANICH ROAD
SIDNEY BC V8L 4B2

8. PERFORMING ORGANIZATION REPORT NUMBER

9. SPONSORING/MONITORING AGENCY NAME(S) AND ADDRESS(ES)
Office of Naval Research
ONR 252 : Diane Gales
Ballston Centre Tower One
800 N. Quincy Street, Arlington VA 22217-5660

10. SPONSOR/MONITOR'S ACRONYM(S)

11. SPONSORING/MONITORING AGENCY REPORT NUMBER

12. DISTRIBUTION AVAILABILITY STATEMENT
Approved for Public Release; distribution is Unlimited

13. SUPPLEMENTARY NOTES

14. ABSTRACT
This experiment was designed to assess the role of bubbles in modifying the high frequency acoustic properties of the near surf environment. The observations included measurement of bubble size distributions in the surf zone and also on a frame deployed offshore by NRL, together with turbulence, wave elevation, 100 kHz propagation, acoustic Doppler, bubble imaging and related environmental measurements.
This extensive data set has provided a basis for detailed modeling of the bubble advection by currents, redistribution by bottom generated turbulence, dissolution and modification by buoyancy effects. The results are compared with measured bubble populations at the NRL site and provide a means for deriving acoustical properties of the water column. In particular, the acoustical attenuation associated with bubbles is derived at two different frequencies.

15. SUBJECT TERMS

16. SECURITY CLASSIFICATION OF:			17. LIMITATION OF ABSTRACT	18. NUMBER OF PAGES	19a. NAME OF RESPONSIBLE PERSON
a. REPORT	b. ABSTRACT	c. THIS PAGE	UU		DAVID FARMER
					19b. TELEPONE NUMBER *(Include area code)* 250-363-6788

significant number of bubble populations during some rip current events. ***Since bubble size distributions are crucial to understanding high frequency propagation, the size distribution is the primary focus of this initial part of our research.***

Our experiment was carried out in the surf zone next to Scripps' Pier at Scripps Institution of Oceanography, La Jolla, California in March 1997 in collaboration with researchers from Naval Research Laboratory (NRL), Stennis Space Center, Mississippi, Scripps Institution of Oceanography, California, Applied Physics Laboratory (APL) in Seattle and the Institute of Ocean Sciences, BC, Canada.

The data presented are interpreted with the use of a simple model which includes bubble buoyancy and dissolution as well as realistic turbulence, rip current speeds and surface wave field.

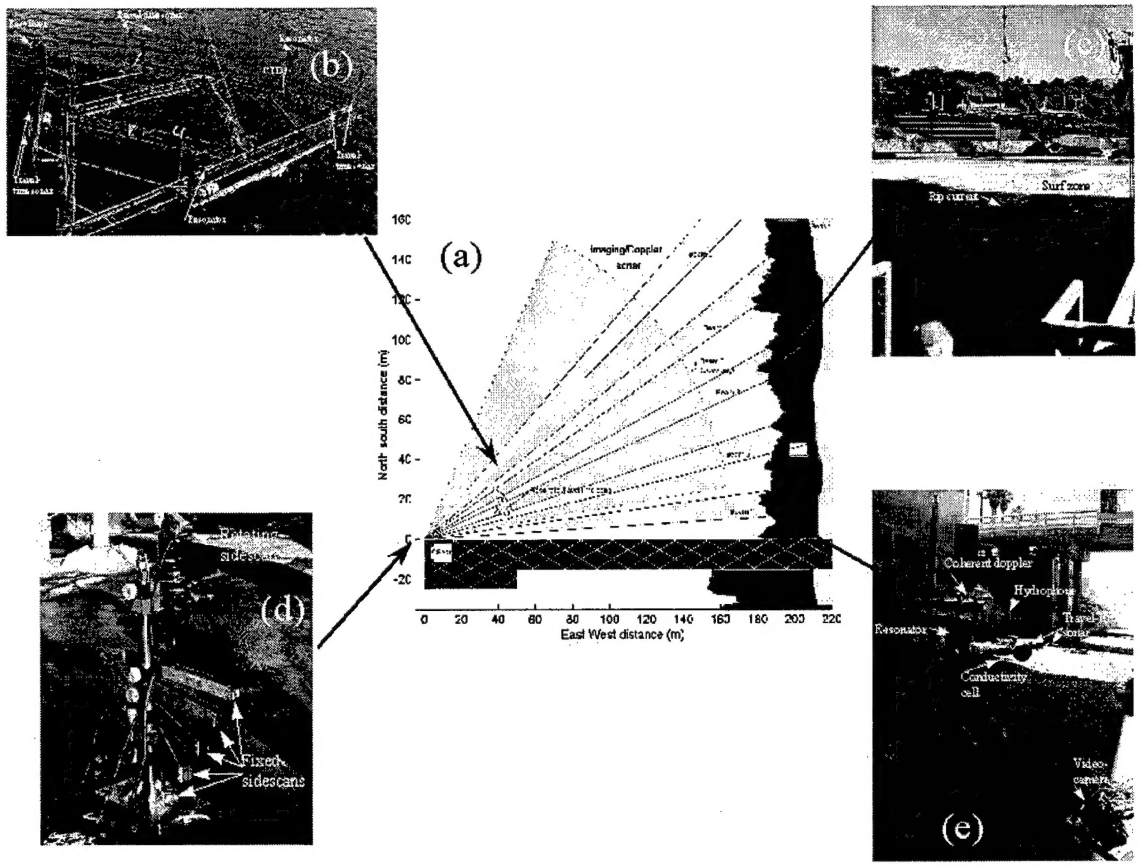

Figure 1. Schematic diagram of experimental site showing the location and look of each instrument.

Measurement Approach

A number of physical parameters are required to understand offshore bubble transport from the wave breaking source in the surf zone and offshore. It is necessary to measure the size distribution, air-fraction and air saturation levels at the source, the long-shore currents and associated turbulence moving the bubbles parallel to the shore towards the region of the offshore rip current. In the rip-current the magnitude of the flow is required as well as the turbulent velocity field within the current itself; finally the bubble size distribution will have to be measured at offshore locations for verification. The turbulence associated with the rip current is controlled by bottom topography and roughness, the surface wave field and the rip current velocity as well as the relative direction between the wave field and current.

During the Scripps experiment a number of the required parameters were sampled using a range of different sensors. The missing variables were obtained from the literature and from numerical models as discussed below.

Bubble size distribution at source

Direct measurements in the surf zone were made from sensors mounted on a steel frame jetted into the sand at low tide (Fig. 1(d)). The bubble size distribution and concentration at the source was obtained from three different types of sensors. The first was an acoustical resonator (Farmer et al., 1998) which measures the attenuation and sound speed changes caused by a distribution of bubbles moving through the insonified volume between two steel plates. This device measures the bubble size distribution at up to 40 frequencies, or bubble radii, between 5kHz (650 μm) and 180kHz (18 μm) at a rate of 2Hz. The second device is a pulse propagation sonar which measures the attenuation and sound speed by transmitting short pulses over a known distance. The third method uses a conductivity sensor to obtain the total air-fraction at high bubble concentrations. A comparison of these methods and their strengths and weaknesses are reported by Vagle and Farmer (1998). The depth of these sensors varied between 0.1 and 1m depending on the tide. The surf frame was also equipped with a video camera, hydrophone, temperature sensor and coherent Doppler system for local turbulence measurements.

Bubble transport

The transport of bubbles in the surf zone and rip currents was tracked using 100kHz sidescan sonars mounted at the end of the pier pointing towards shore. Five transducers were mounted as shown in Fig. 1(b,e) each pointing in a different direction every 10^o with 2^o (3dB) beam-widths. This system was sampled at 2Hz and transmitted 32 bit Barker codes for calculations of Doppler velocities as well as the backscattered amplitude. The backscatter amplitude data were used to determine the exact bubble injection time of any particular bubble plume as it moved offshore. No direct measurements were made of the long-shore currents but the Doppler velocities from all

five sonars were used to obtain an estimate of the mean current parallel to the beach. These Doppler measurements were also used to track and measure the mean velocity of the rip currents. In addition to the five fixed transducers a sixth was swept in a 50^o sector every 30 seconds to obtain an overview of the spatial distribution of the bubble field in the area. The raw backscatter data were also used to track the surface wave field by utilizing the Doppler signal from the particle trajectories under the waves.

Bubble measurements outside the surf zone

As part of the Scripps 97 experiment NRL deployed a triangular frame (Delta frame) with 10m sides on which were mounted a number of sensors for acoustical propagation studies. We also installed three acoustical resonators and two pulse propagation sonars along the three legs of the frame (Fig. 1(a)) These sensors sampled the bubble field at 1 Hz and measured bubbles with radii ranging from 18 to 500 μm. This frame was deployed ca. 45m from the end of the pier (Fig. 1(e)), well outside the surf zone, and our sensors were located at a mean depth of 3.5m in waters with a mean depth of 5m.

Models of Offshore Bubble Transport and Turbulence

The model used here to tie together the different measurements described in the previous section is based on the one developed by Thorpe (1982). In this model both bubble buoyancy and dissolution have been incorporated. Our interest in dissolution in the present context arises from its potential importance in turbulent fields where the bubbles are drawn down to considerable depths. Since turbulence plays a major part in the dynamics of the surf zone we have chosen to incorporate a vertical turbulent velocity using one of the eddy viscosity models described by Christoffersen and Jonnson (1985).

Bubble advection and dissolution

Bubbles in natural water rapidly acquire surface-active materials onto their surface modifying their rise speed as well as the gas diffusion rate and acoustic properties. This causes them to behave like rigid bodies. Thorpe (1982) called these bubbles "dirty" to distinguish them from bubbles without any surface-active coating which he called "clean". Clean bubbles will become dirty within tens of seconds (Thorpe, 1982) in normal sea water making it appropriate to consider dirty bubble characteristics only.

For simplicity we assume the bubbles are composed solely of oxygen. However it would be straight forward to add the extra terms associated with a more realistic bubble gas composition which includes nitrogen. The ratio of oxygen to nitrogen is approximately 7:26 at the ocean surface. Wyman et al. (1952) obtained a relationship between the mole fraction of oxygen , M , in the bubble and its size, temperature and pressure as

$$M = \frac{4\pi a^3}{3RT}\left(p + \frac{2\gamma}{a}\right) \quad , \tag{1}$$

where a is the bubble radius, p is the hydrostatic pressure, T is the temperature (K), R is the gas constant ($m^3kPaK^{-1}mol^{-1}$) and γ is the surface tension. An assumption here is that the water is isothermal and that the gas temperature is the same as that of the water. Gas will invade or escape from the bubble according to the Nusselt number, Nu, which is assumed independent of fluctuations in the hydrostatic pressure (Thorpe, 1982). At high Peclet number, Pe, (radii greater than approximately 20 μm), but small Reynolds number Levich (1962) found that for "dirty" bubbles,

$$Nu = \frac{Q}{4\pi aD(C - C_\infty)} = \left(\frac{2}{\pi}\right) Pe^{1/3}, \tag{2}$$

with D being the diffusivity of oxygen in water, Q is the rate of transfer of gas from the bubble surface, C the concentration of gas in the bubble, C_∞ the concentration in the water far from the bubble, and

$$Pe = \frac{aw_b}{D}, \tag{3}$$

where w_b is the bubble rise speed due to buoyancy. The concentrations, C and C_∞ can also be expressed in terms of the coefficient of gas absorption, κ, as

$$C = \kappa P \tag{4}$$

and

$$C_\infty = \kappa P_\infty \tag{5}$$

where P and P_∞ are the partial pressures of oxygen in the bubble and in the surrounding water respectively.
Based on equations (2), (4) and (5) one can obtain

$$\frac{da}{dt} = \frac{-1}{(3p + 4\gamma / a)} \left\{ \frac{3RT}{a} \left[D\kappa (Nu) \left(\left(p + \frac{2\gamma}{a} \right) - P_\infty \right) \right] + a \frac{dp}{dt} \right\}, \tag{6}$$

which represents the time rate of change of bubble radius as a result of gas diffusion and changing hydrostatic pressure.

The possibility of growth in size of the bubble by coalescence with other bubbles has been ignored as justified by Thorpe (1982). Memery and Merlivat (1985) show that surfactants on the bubbles can reduce the gas exchange by a factor of five. However, this is still an issue under investigation and in the present study we will assume that (6) is valid in its present form.

Bubbles in water will rise due to their buoyancy at a speed w_b. If the water surrounding a given bubble is moving vertically with a random turbulent velocity w, the actual descent rate will be

$$\frac{dz}{dt} = w - w_b \quad , \tag{7}$$

or

$$\frac{dp}{dt} = g\rho(w - w_b) \quad , \tag{8}$$

where $p = p_0 + g\rho d$ is the pressure in the water at depth d, the surface pressure is p_0, g is the gravitational acceleration and ρ is the water density.

The terminal velocity of a bubble can be obtained from the balance between drag and buoyancy forces

$$C_D \frac{\pi a^2}{2} \rho w_b^2 = \rho g \frac{4\pi}{3} a^3 \quad , \tag{9}$$

where a is the bubble radius and C_D is a drag coefficient. Keeling (1993) defined C_D in terms of the Reynolds number Re as

$$C_D = \frac{24\,\mathrm{Re}}{1 + 0.566\,\mathrm{Re}^{0.5}}, \tag{10}$$

where

$$\mathrm{Re} = \frac{2aw_b}{\nu} \tag{11}$$

and ν is the kinematic viscosity of the water. For bubbles with radii greater than $560\mu m$ the rise speed is assumed to be constant (0.3m/s) (Levich, 1962).

The turbulent vertical flow velocity w in (7) and (8) was not measured during the present study. We use information from the literature to obtain an appropriate model for the conditions encountered here.

Turbulent vertical velocity component w

In the surf zone and within rip currents, bottom boundary layer turbulence is generated by both surface waves and more steady motions such as the flows associated with long-shore and rip currents. It is well known (e.g., Lundgren, 1972; Smith, 1977) that a result of the momentum flux from the fluid to the sea bed is that the surface waves and currents are coupled through the sea bed shear stress. Several theories and models have been developed based on this fact for the combined-flow boundary layers (Grant and Madsen, 1979 ; Christoffersen and Jonsson, 1985) and all would probably be suitable for the present work. However, we have chosen to use one of the two models described by Christoffersen and Jonsson (1985) because of the well written recipe for its coding and use.

The model is based on the assumption that the offshore rip current is steady and that the sea bed is locally horizontal. In addition lateral shear stresses in vertical sections as well as Coriolis and tidal forces are neglected. The model calculations are based on the following nine equations

$$f_c = \frac{2}{\frac{1}{\kappa}\left(\ln\frac{30h}{ek_N} - \ln\frac{k_A}{k_N}\right)}, \tag{12}$$

$$J = \frac{0.273313am\sqrt{gk\tanh(kh)}}{\sinh(kh)k_N\omega_a}, \tag{13}$$

$$f_w = \frac{0.1494m}{J}, \tag{14}$$

$$\sigma = \frac{f_c}{f_w}\left(\frac{U\sinh(kh)}{a\sqrt{gk\tanh(kh)}}\right)^2, \tag{15}$$

$$m = \sqrt{1+\sigma^2+2\sigma|\cos(\alpha)|}, \tag{16}$$

$$\delta_w = 0.1229908k_N\frac{\pi}{2}\sqrt{J}, \tag{17}$$

$$k_A = 30\delta_w\exp\left(-\frac{\kappa}{0.0747}\frac{\delta_w}{k_N}\sqrt{\frac{\sigma}{m}}\right), \tag{18}$$

$$u_{fc} = \sqrt{\frac{1}{2} f_c U}\,, \tag{19}$$

and

$$u_{fm} = \sqrt{\frac{1}{2} m f_w}\,\frac{a\sqrt{gk\tanh(kh)}}{\sinh(kh)}\,. \tag{20}$$

In equations (12) to (20) f_c and f_w are current friction and wave friction factors for combined current wave motion, h is the mean water depth, $\kappa = 0.40$ is the Karman constant, $e = \exp(1) = 2.718....$, and k_N and k_A are Nikuradse (geometrical) and apparent bottom roughness. Because of the Wave Boundary Layer (WBL) the current meets a greater bed shear than a pure current and therefore will experience a greater, apparent, roughness than the Nikuradse roughness. Furthermore, a is the wave amplitude, g is the gravitational acceleration, $k = 2\pi / L$ is the wave number with L being the surface wave length, $\omega_a = 2\pi / T_a$ where T_a is the absolute wave period, α is the relative angle between the direction of the current and the incoming wave field , U is the magnitude of the average-over-depth current velocity, δ_w is WBL thickness and u_{fc} and u_{fm} are the current and maximum friction velocities, respectively.
Christoffersen and Jonsson (1985) went on to define the time independent eddy viscosity K as a WBL eddy viscosity K_w and a current boundary layer eddy viscosity K_c

$$K_w = 0.0747 k_N u_{fm} \qquad 0 \le z \le \delta_w \tag{21}$$

and

$$K_c = \kappa z\left(1 - \frac{z}{h}\right) u_{fc} \qquad \delta_w < z \le h\,. \tag{22}$$

With knowledge about the mean water depth, h, the surface wave field (a, T_a, L), the rip current velocity U, the relative direction between this current and the wave field α and the bottom roughness, k_N, the eddy viscosity at any given depth can be obtained from solving equations (12) to (22). The procedure is to calculate f_c from (12) assuming $k_A = k_N$, initially. Calculate J and f_w (Equations (13) and (14)) using $m = 1$. Keeping f_c fixed iterate through equations (15) (16) (13) and (14) until sufficient accuracy is obtained for σ, m, J and f_w. Calculate δ_w and k_A using (17) and (18). Compute a new f_c value using (12) and repeat the sequence until desired accuracy in f_c. Finally the eddy viscosity profile is calculated using Equations (19) to (22). An example of a typical eddy viscosity profile from this model is shown in Figure 2.

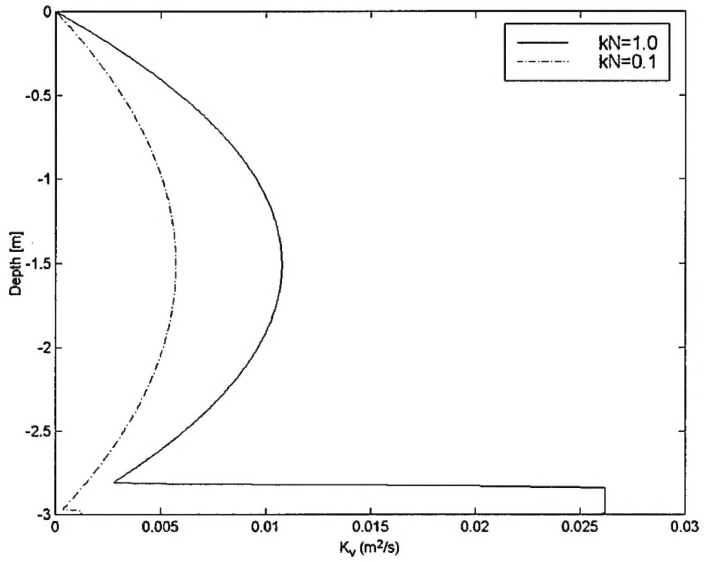

Figure 2. Typical eddy viscosity profiles at different bottom roughnesses from Christoffersen and Jonnson (1985) model

The eddy viscosity can be related to a maximum turbulent velocity $w_{\max}$ using

$$w_{\max} = 2\sqrt{\frac{K}{\Delta t}} \tag{23}$$

where Δt is a typical time scale, or in the case of a numerical model it represents the time step of the calculations. To represent this turbulence in our model w is randomly chosen between $-w_{\max}$ and $+w_{\max}$.

Model implementations

When dealing with advection of bubbles by a time and space independent rip current one can use both the time t, since bubble generation, and distance away from the source region x, as independent variables. The transformation between them is

$$x = Ut\,. \tag{24}$$

Equations (6), (7) and (8) were solved numerically using a 4th Order Runga Kutta method from $t = 0$ to $t = t_t$ with an initial bubble size distribution as a function of depth. The equations were solved for each depth and each bubble size increment individually and added to the individual bubble radius and depth bins at $t = t_1$. The randomness of the vertical particle velocity was incorporated by obtaining an ensemble average over a number of different model runs.

The bottom bathymetry which constrained the geometric boundary condition was obtained from Terrill (1998) for the period considered here. Finally, the eddy viscosity field was calculated for each time step by transforming to range space using (24) and calculating the local eddy viscosity profile from Equations (12) to (22) using the correct water depth and surface wave field parameters at each location x. An example of such a field is shown in Figure 3.

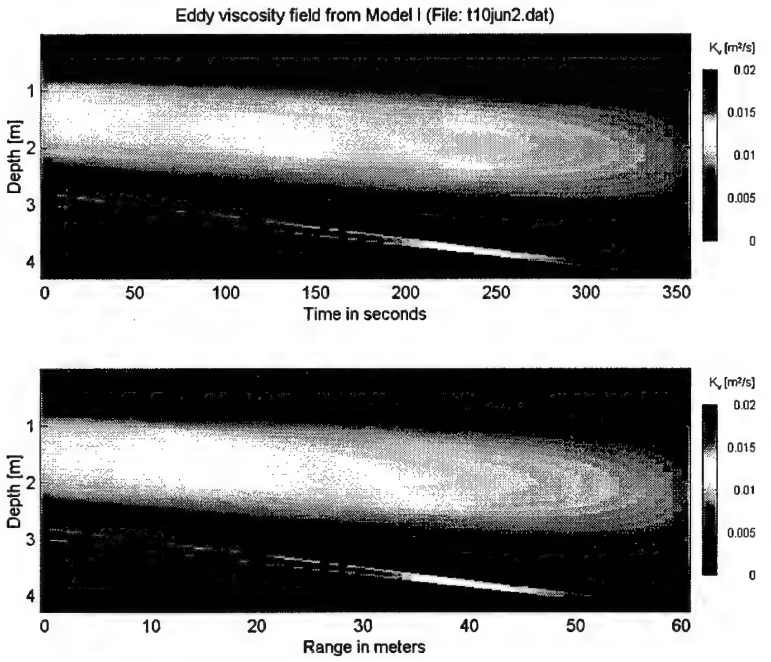

Figure 3. Eddy viscosity field for bathymetry and geometry at Scripps.

Observations

The bubble size distribution in the surf zone was measured using an acoustical resonator mounted on a frame jetted into the sand as described earlier (Fig. 1(d)). For strong events, when the air-fraction was higher than approximately 10^{-4}, the conductivity sensor on the same frame was used to obtain the total air-fraction. Figure 4 shows a series of four photographs of an approaching spilling breaker. The surf frame can be spotted slightly to the right of the center in the images. The top panel shows the measured air-fraction during this event. The air-fraction increases rapidly to more than 2% as the wave crest reaches the frame, followed by a rapid decay over the next second, followed by a more gradual decay. It is worth noting that this particular measurement technique is very sensitive to temperature and salinity variations at air-fractions less than approximately 10^{-4}. At these lower levels the resonator data were used to obtain the bubble size distribution and the total air-fraction.

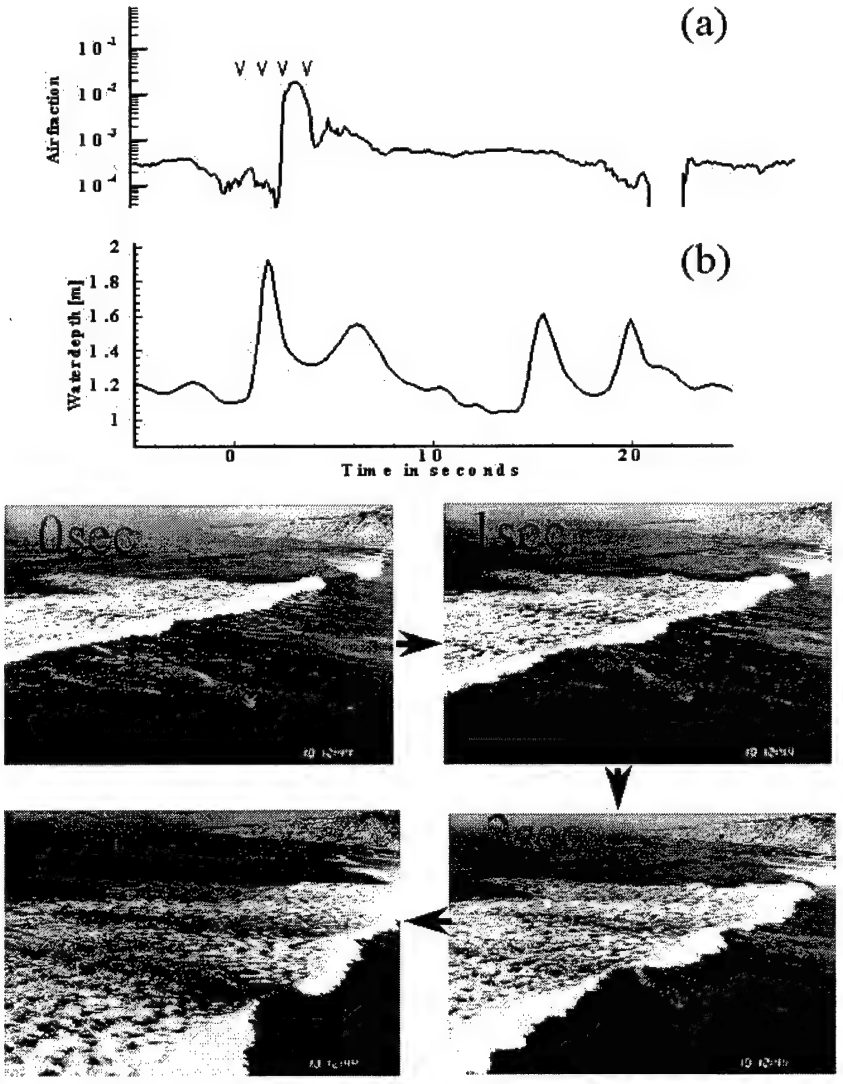

Figure 4. Photographs of approaching spilling breaker. Surf frame shown right of center of photos. Upper panel shows the air-fraction as observed with a conductivity sensor mounted on the frame (a) and the surface elevation as measured with a pressure sensor on the frame (b).

One such smaller event is shown in Figure 5. Here the air-fraction increases by 5 orders of magnitude to more than 10^{-4} as the bubble plume passes the sensor, followed by a slow decay (Fig. 5(a)). This decay time is typically 300 to 400 seconds for the events observed in this study. Six bubble size distributions selected at times indicated in Fig. 5(a) are shown in Fig. 5(b). One can see the presence of significant numbers of large ($> 200\mu m$)

and smaller bubbles ($< 30\mu m$) during the initial stages of the event followed by a rapid decrease in the number of both small and large bubbles, especially the largest bubbles. As will be shown later, this evolution relates to the buoyancy of the larger bubbles and dissolution of the smallest ones. This change in shape of the bubble size distribution is even more obvious in Fig 5(c) where the size distributions have been scaled by volume ($4/3\pi a^3 n(a)$). The slope of the size distribution shortly after passage of the plume is close to radius^{-2}, as indicated in the figure. This is the shape of the bubble size distribution used as the source distribution in the numerical model described previously.

The sensors on the surf frame could only be used within ±1h of high tide because of the requirement that all sensors be submerged during a wave cycle. Unfortunately, all rip-current events observed by the 100kHz sidescan sonar system and by sensors on the NRL Delta frame occurred during, or close to, low tide. This constraint was imposed by the maximum depth at which the frame could be deployed. It is therefore not possible here to track an individual bubble plume directly from the source breaking wave and out to the sensors outside the surf zone. Instead we have to determine the location and start time of a rip-current event from the 100kHz sidescan sonar data and assume that the bubble size distribution and total air-fraction at the source is similar to the breaking events during high tide. This is a reasonable assumption since the slope of the sea floor is fairly constant ( ), so that tidal phase primarily alters the location rather than the character of the surf zone.

The averaged (20 sec.) backscatter amplitude signal from sidescan sonar beam 2 (Fig 1) for a one hour period has been plotted in Fig.6(a). Large amplitudes, or dark patches, indicate regions with large backscatter and presumably high bubble concentrations. These data are from a low tide period in which one can see that the surf zone is located between 90 and 120m from the end of the pier. (For comparisons it is worth noting that our surf frame was located approximately 220m from the end of the pier and therefore dry during this particular period.) The high backscatter sections at a range of approximately 100m from the sonar are presumably due to bubble injections by breaking waves or bubble plumes advected by long shore currents into the sonar beam. The tilted, more narrow, bands between 100m and 40m are caused by offshore currents pulling bubbles away from the breaking zone. Figure 6(b) shows the total air-fraction measurements at a depth of 3.5m and range of 45m from the end of the pier (broken line in Fig. 6(a)). One can see that of the two major rip-current events during this period only one shows significant bubble concentrations at the sensor outside the surf zone. The speed of these rip-currents

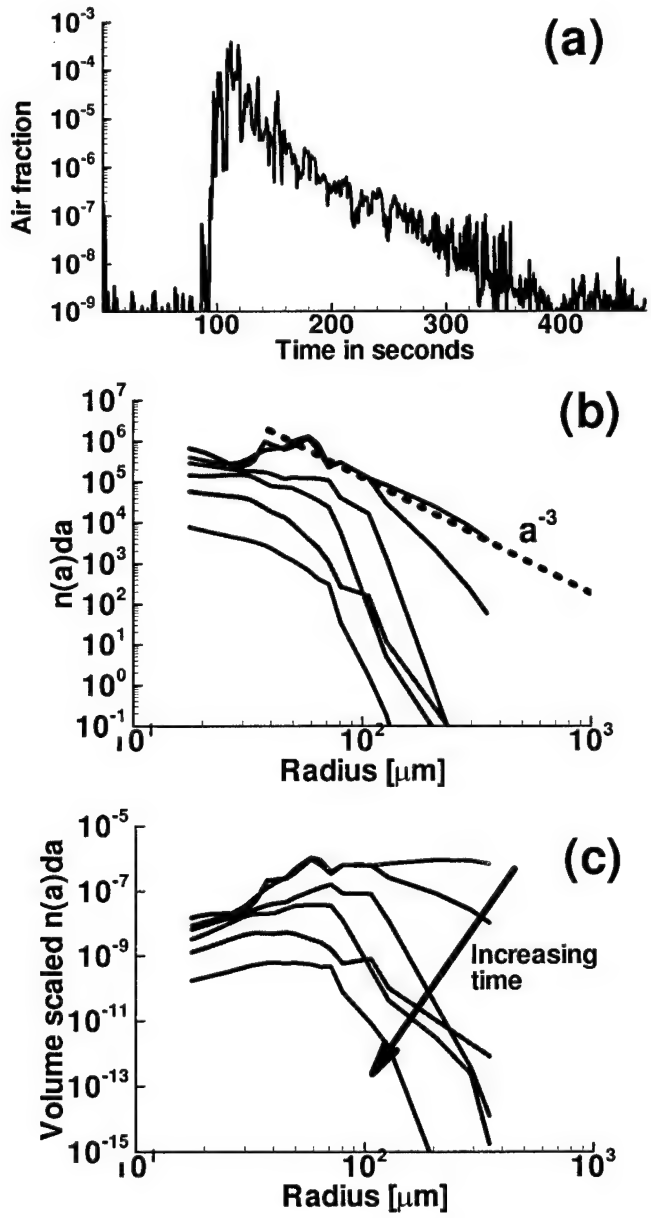

Figure 5. Air-fraction from resonator for smaller event in the surf zone at a depth of 1m (a) and corresponding bubble size distributions (b) and volume scaled size distributions (c).

can be estimated from the slope of these lines or from the Doppler velocity measurements obtained from the same backscattered signals.

Based on the Doppler measurements as well as the slopes of the coherent bands in time versus range versus amplitude plots, the rip-current speeds were found to vary between 5 and 40cm/s with slightly more variability in the beginning of the experimental period when the significant wave height was high relative to the end of the period when the surface wave field was very weak (Fig. 7).

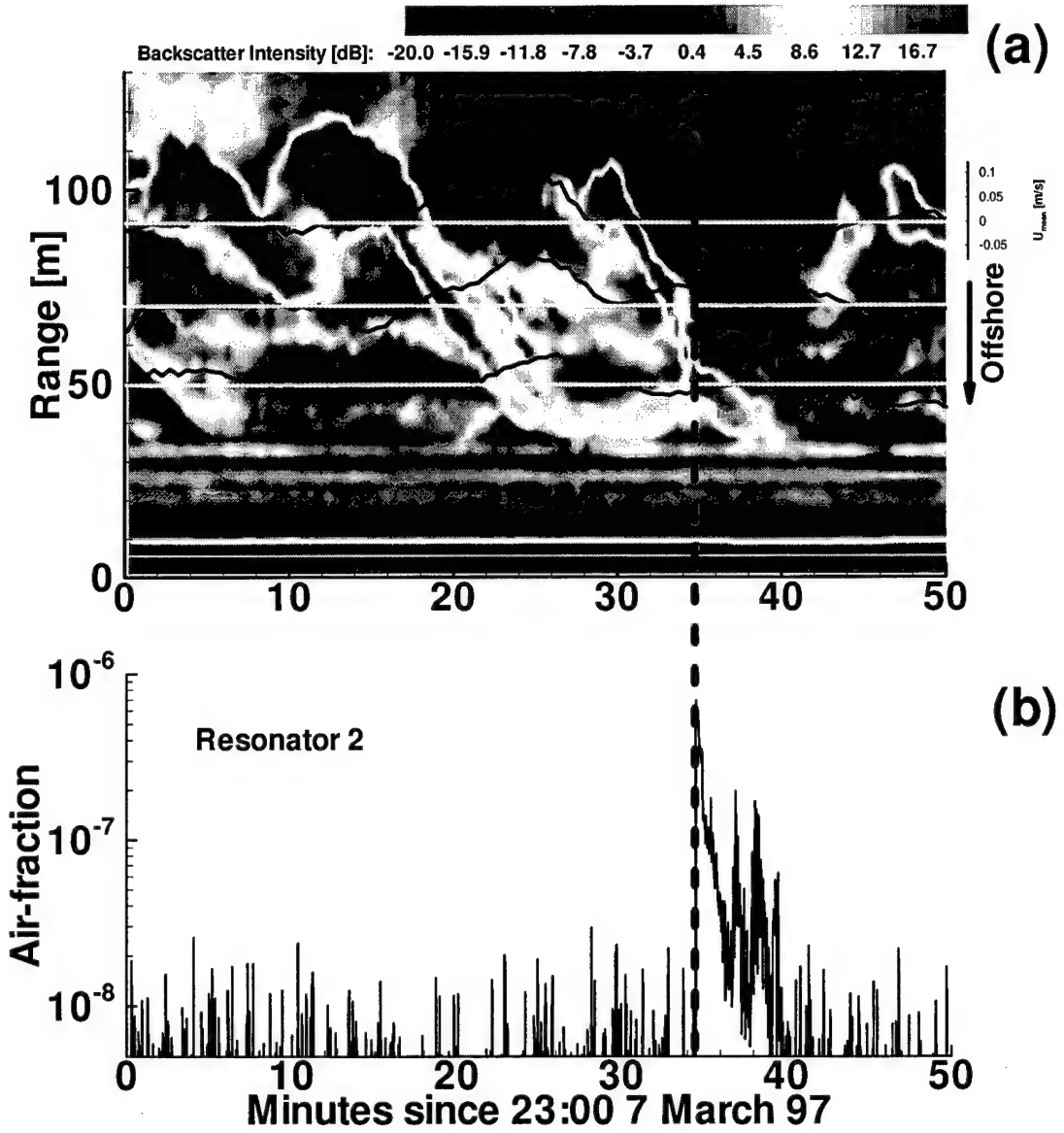

Figure 6. Contour plot of 20 second averaged 100kHz sidescan beam 2 backscatter amplitude data during a low-tide period with rip-current events and the corresponding offshore current speeds at three ranges as obtained from the Doppler measurements (a). The lower panel (b) shows the total air-fraction as measured with a Delta frame mounted resonator at a range of 40 m and depth of 2.5m.

From some simple correlation studies between the 100kHz backscatter amplitude data, video recordings from the pier and the surf frame sensors it was difficult to find any simple correlation between the different measurements. It is clear from the video footage that there are many more wave breaking events per hour than the four to five distinct events showing up in the backscatter amplitude data. We hypothesize that wave breaking is taking place all the time in the surf zone parallel to the beach, feeding bubbles into the long-shore currents which control the gross features of the bubble field. And it is

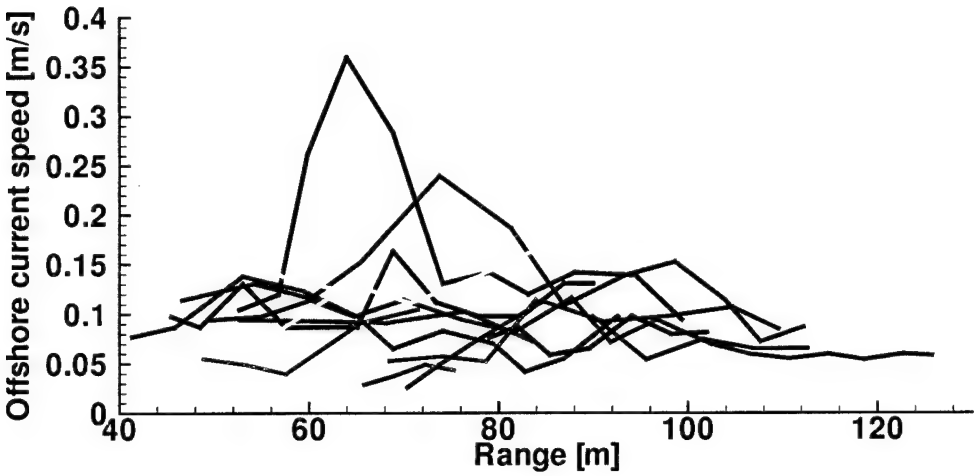

Figure 7. Mean, maximum and minimum rip-current speeds as measured during each low-tide period during the experimental period (a) and rip-current speeds along the path of the currents for a number of observed rip-currents (b).

these gross features we are observing in the sidescan data. Since no direct measurements of the long-shore flow were made during the experiment we used the Doppler velocities from the five fixed sonar beams to decompose the measured velocities into an offshore and long-shore component.

The short term averages (1-2 sec.) of the 100kHz Doppler velocity data clearly show the signature from surface gravity waves approaching the beach (Fig. 8). Acoustical energy is scattered from bubbles following the orbital motion of the waves; the observed velocities are most likely associated with wave troughs and not crests. For the present purpose we only need an approximate knowledge of the wave field in terms of the wave period to obtain the required parameters for the eddy viscosity model discussed in the previous section. Here we use shallow water theory and prior knowledge of the bathymetry to calculate the wave amplitude and length as a function of range from the surf zone. Based on video and other visual observations we are assuming that the incoming surface gravity waves and outgoing rip-currents are directly opposing each other ($\alpha = 180^o$).

The acoustical bubble sensors on the NRL Delta frame only detected bubbles during low, or close to low, tide at threshold levels of approximately 10^{-9}. Even at low tide and with clear rip-current signature on the 100kH sidescan channels only a few were detected at the Delta frame sensors. Over the 10 day duration of the experiment approximately 1 in 3 resulted in bubbles at these sensors. This suggests that some of the rip-currents were relatively shallow or that the bubbles had gone into solution or risen to the surface by the time they reached the frame. The sensors were mounted at a mean depth of 2.5m. Figure 10 shows the total air-fraction and associated bubble size distributions for the three resonators during one detectable event. The event is the one shown in Figure 6 at 23:30

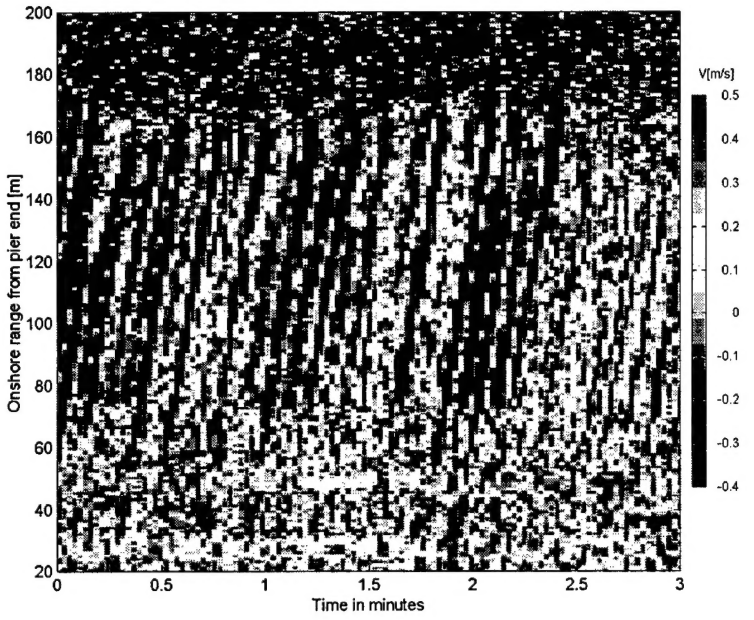

Figure 8. An example of 1.5 second averaged Doppler velocity data showing the orbital particle velocity associated with approaching surface gravity waves.

to 23:40. At this time the total air-fraction has dropped by 4 to 5 orders of magnitude from the levels observed in the surf zone. Differences in the total air-fraction at the three different sites also show the large spatial and temporal variability in the bubble field. Figure 10(b) and (c) show the actual and volume scaled bubble size distributions at the times shown in Fig. 10(a) for sensor 2, which was closest to shore. It is clear that the large bubbles have risen to the surface, explaining the large drop in air-fraction.

The backscatter data in Fig. 6(a) suggest that the bubble plume originated from a location 55m further offshore where it appeared approximately 5 minutes earlier. The fact that the number of bubbles smaller than $20\mu m$ remains relatively high suggests that the oxygen saturation level in the water is high, keeping these bubbles from going into solution.

Model Simulations

The surf zone bubble model described in equations (1)-(23) above has been implemented for a range of parameters applicable to the experiment. Key variables include a supersaturation level of 20% for oxygen, 10% for nitrogen, initial air-entrainment fraction in the breaking wave of 0.1% and initial bubble cloud depth of 3m. A depth bib of 0.1m was used in the calculations which spanned bubble radii of 10-1000 microns having an initial power law size distribution of -3. The calculations used a time step of 1s. Figure 9 shows a result of this particular run, including air-fraction, the acoustic attenuation at 12kHz and the acoustic attenuation at 50kHz.

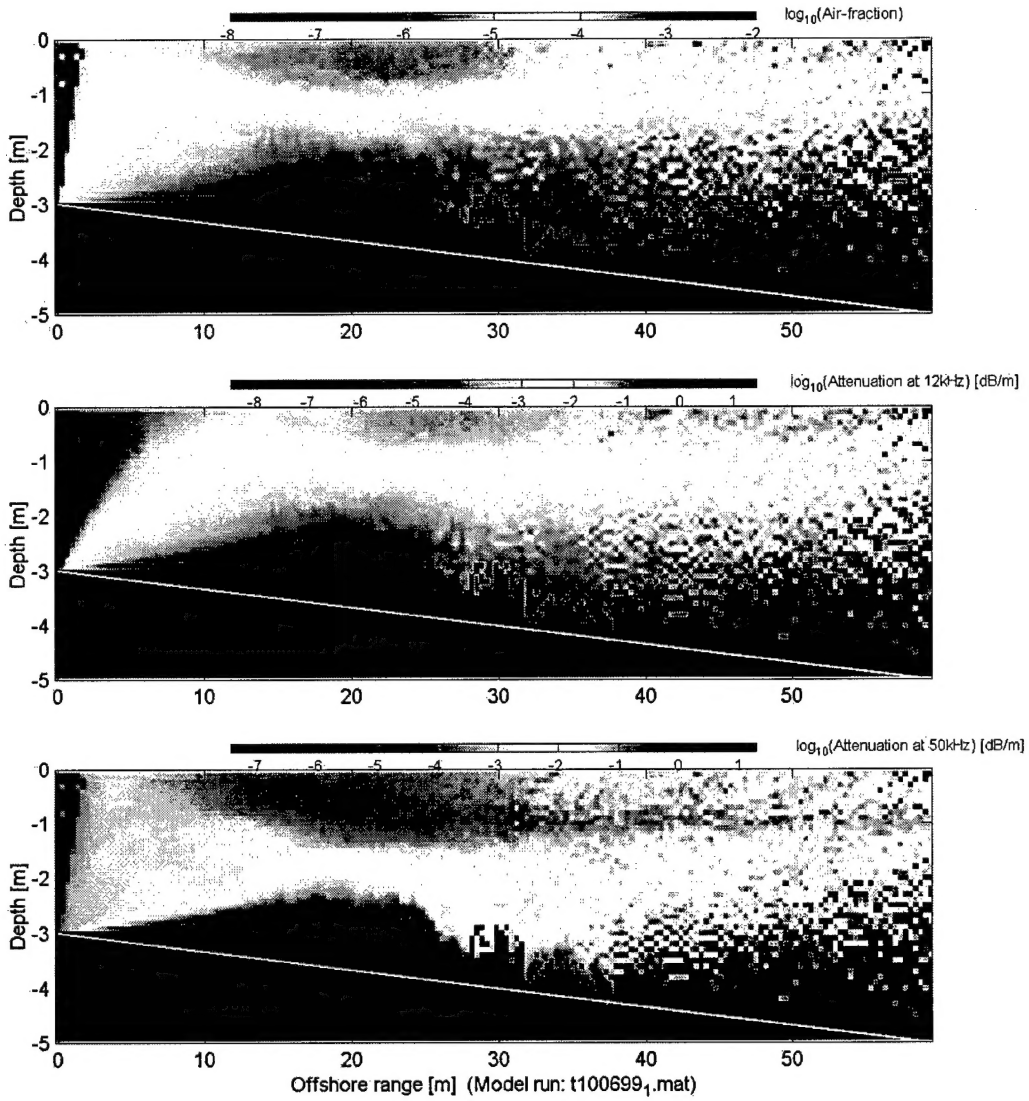

Figure 9. Modeled air-fraction (top) and acoustic attenuation at 12kHz (middle) and 50kHz (bottom). The air fraction is modeled on the basis of observed injection characteristics and rip tide current, with calculated turbulence diffusion, buoyancy and dissolution. The calculation represents an integral over all bubble sizes.

The upper frame of Fig. 9 illustrates the inshore boundary condition (bubble supply) in the breaking wave zone. The combined effects of buoyancy, advection, turbulence and dissolution combine to form a greater concentration of air near the surface between 10 and 30m offshore of the breaker zone. Much lower concentrations of bubbles can penetrate close to the sea floor at ranges of 30-50m, consistent with the occasional measurements of bubbles on the NRL Delta Frame. From an acoustic propagation point of view, the bubble size distribution is of particular interest, since attenuation due to bubbles is sharply peaked at the resonant frequency. Evaluation at particular frequencies can be carried out by integration over all radii present. The calculations in Figure 9 (middle frame) are evaluated for 12kHz. Away from the bubble source, maximum attenuation occurs close to the surface. This can be explained by the importance of buoyancy to the larger bubbles which attenuate the lower frequencies.

Subtle but potentially important differences occur at higher frequencies. At 50kHz, high attenuation occurs close to the surface between 10 and 35m range and over the upper 1.5m. But further offshore the attenuation maximum is displaced beneath the surface. The explanation must be sought in the competition between turbulence, which redistributes the bubbles vertically, and the loss of bubbles near the surface through buoyancy effects. The turbulence in this case is generated over the sea floor and therefor decays nearer the surface, allowing buoyancy to more effectively remove near-surface bubbles. At slightly greater depths, the concentration of resonant bubbles increases.

Conclusions

The Scripps bubble experiment provided us with a unique opportunity to acquire measurements of wave breaking, bubble clouds, currents and bubble size distributions in the surf zone, all relevant to acoustic propagation. It must be emphasised that this represents just the first step in a comprehensive inshore propagation model. The bubble model is crucial because the bubbles produce a dispersive layer that varies greatly with frequency. Ultimately, any satisfactory acoustic model will have to account for both real and imaginary components of the dispersion. Within the limits of the present contract we have demonstrated the general properties of the bubble field as it evolves under the influence of rip currents, wave induced turbulence, bubble buoyancy and the differential dissolution of nitrogen and oxygen. We have also calculated the resultant attenuation of 12kHz and 50kHz signals. A full discussion of the acoustic implications is a matter for continuing and active research, but will in any event depend for input on the results of the observations and model calculations provided here.

References

Christoffersen, J.B., and I.G Jonnson, 1985, Bed Friction and Dissipation in a Combined Current and Wave Motion, *Ocean Engng*, Vol.12., No. 5, pp 387-423

Dyhr-Nielsen, M., & Sorensen, T., 1970, Sand transport phenomena on coasts with bars. *Proc.12th Coastal Engng. Conf.*, pp. 855-66

Farmer, D.M., Vagle, S., & A. D. Booth, 1998, A free flooding acoustical resonator for measurement of bubble size distributions, ***J. Atmos. & Oceanic Technol.***, Vol. 15, No. 5, pp. 1132-1146.

Grant, W.D, and Madsen, O.S., 1979, Combined wave and current interaction with a rough bottom., *J.Geophys. Res*, 84 (C4) 1797-1808

Levich, V.G., 1962, *Physico-chemical hydrodynamics*. New York: Prentice-Hall

Lundgren, H., 1972, Turbulent currents in the presence of waves. *Proc. 13th Coastal Engng Conf., Vancouver 1972*, Vol. 1. Pp. 623-634, Am.Soc. Civ. Engrs. New York.

Memery, L., and Merlivat, L., 1985, Modelling of gas flux through bubbles at the air-water interface. *Tellus* 37B, 272-285

Smith, J.D.,1977, Modeling of sediment transport on continental shelves. In *The Sea*. Vol. 6. Edited by Goldberg, E.D., McCave, I.N., O'Brien, J.J. and Steele, J.H. Wiley-Interscience. New York.

Thorpe, S.A., 1982, On the clouds of bubbles formed by breaking wind-waves in deep water, and their role in air-sea gas transfer.

Vagle, S. & D.M. Farmer, 1998, A Comparison of four methods of bubble measurement, ***IEEE Oceanic Engineering***, v 23, No 3, 211-222.

Wyman, J., Scholander, P.F., Edwards, G.A. & Irving, L., 1952, On the stability of gas bubbles in sea water. *J.Mar.Res*. 11, 47-62.